PERGAMON

International Journal of Heat and Mass Transfer 42 (1999) 1555–1568

International Journal of HEAT and MASS TRANSFER

Comparative analysis of jet impingement and microchannel cooling for high heat flux applications

D.-Y. Lee[a], K. Vafai[b,*]

[a] *Korea Institute of Science and Technology, Seoul 130-650, Korea*
[b] *Department of Mechanical Engineering, The Ohio State University, Columbus, OH 43210, U.S.A.*

Received 12 February 1998; in final form 14 August 1998

Abstract

In this work, a comparative investigation of jet impingement and microchannel cooling is presented. The thermal performance of each technology evaluated at the respective optimal condition is compared to each other with the target dimension as a main parameter. It is revealed that the microchannel cooling is preferable for a target dimension smaller than 0.07 by 0.07 m, while the jet impingement is comparable or better than the microchannel cooling for a larger target plate if a proper treatment is applied for the spent flow after the impingement. Various pertinent aspects of each technology as well as a detailed comparative analysis of the two technologies are presented. In selecting a technology from the two, the economic aspects, such as manufacturing and maintenance cost, also have to be taken into account, since the better performing one may not be necessarily the more suitable one.

Nomenclature

A surface area of the target plate [m^2]
A_{corr} surrounding area corresponding to a single jet [m^2]
a_1, a_2 exponents in equations (51) and (52)
C_D orifice discharge coefficient
c_1, c_2 proportional constants in equations (51) and (52)
c_P isobaric specific heat [J kg^{-1} °C^{-1}]
d nozzle diameter [m]
d_h hydrodynamic diameter of microchannel [m]
F Reynolds function
f friction factor, $f = (\Delta p d_h/L)/2\rho u^2$
G geometric function
G_P function defined in equation (26)
H height of the microchannel [m]
h heat transfer coefficient [W m^{-2} K^{-1}]
K jet interaction correction function
k_f thermal conductivity of the fluid [W m^{-1} °C^{-1}]
k_s thermal conductivity of the plate material [W m^{-1} °C^{-1}]
L length of the target plate [m]
m constant defined in equation (55)
n constant defined in equation (55)
Nu Nusselt number, $Nu = hd/k_f$ or $Nu = hd_h/k_f$
P nondimensional pressure loss
P_0 pumping power per unit area of target surface [W m^{-2}]
p pressure [Pa]
Δp pressure difference [Pa]
p_0 pressure in the plenum chamber [Pa]
Pr Prandtl number
Q heat rate [W]
q heat flux [W m^{-2}]
R radius of the target plate [m]
r radial coordinate [m]
Re_J Reynolds number for the jet, $Re_J = u_J d/v$
Re_M Reynolds number for the microchannel, $Re_M = \frac{ud_h}{v}$
S_{NN} nozzle-to-nozzle separation distance [m]
S_{NP} nozzle-to-plate spacing [m]
T temperature [°C]
$T_{f,in}$ fluid inlet temperature [°C]
$T_{f,out}$ fluid outlet temperature [°C]
ΔT temperature difference between the plate and fluid [°C]
t thickness of the target plate [m]

* Corresponding author. Tel.: 001 614 292 6560; fax: 001 614 292 3163; e-mail: vafai.1@osu.edu

0017–9310/98/$ - see front matter
PII: S0017–9310(98)00265–8

u velocity [m s^{-1}]
u_c crossflow velocity [m s^{-1}]
u_J jet velocity [m s^{-1}]
u_J^* artificial jet velocity defined in equation (12) [m s^{-1}]
$\dot{V}$ coolant flow rate [m^3 s^{-1}]
W width of the target plate [m]
w width of the microchannel [m]
x nondimensional radial coordinate.

Greek symbols
α_J relative nozzle area
α_M area enlargement factor in microchannel cooling
ε perturbation parameter in equation (16)
γ ratio of the fin thickness to the microchannel width
η fin efficiency
κ thermal conductivity ratio of plate material to the fluid, $\kappa = k_s/k_f$
λ quantity defined in equation (38)
v dynamic viscosity [m^2 s^{-1}]
Ω quantity defined in equation (47)
θ nondimensional thermal resistance
ρ density of the fluid [kg m^{-3}]
ω pseudo aspect ratio of microchannel
ξ pressure loss coefficient.

Subscripts
cap capacitance resistance
cond conductive resistance
conv convective resistance
fin fin in microchannel
J jet impingement
M microchannel
min minimum
max maximum
opt optimum.

1. Introduction

For many years there has been a growing interest in technologies that include a need to handle significant heat fluxes from or onto surfaces. In many of these cases, the thermal treatment of the high heat duties has been expected to be a major factor which limits further growth in relevant technologies. For example, the effective means of turbine blade cooling has been a primary factor in improving the performance of gas turbines, and the cooling of high heat dissipation electronic components has become a prerequisite to increasing the integration density of microelectronic circuits. More recently the high-heat-flux treatment has also become a crucial technology for the cooling of plasma-facing components in fusion reactors [1] and the cooling of high-power optical components in synchrotrons and power beaming applications [2]. In such applications, the heat flux ranges from a few hundred W cm^{-2} to several thousand W cm^{-2}, which is substantially larger than what can be managed by the usual heat transfer enhancement technologies such as extended or roughened surfaces.

Considerable efforts have been directed toward the development of effective schemes for treatment of high-heat-flux applications. Subsequently, there has been a growing interest in technologies that include a need to handle significant heat fluxes from or onto surfaces, and as such the jet impingement and microchannel cooling have attracted a great deal of attention. While both technologies are known to provide very high heat transfer performance, it is desirable to understand which is preferable for a given high-heat-flux application. In the jet impingement scheme, thin hydrodynamic and thermal boundary layers forming in the impingement region result in high heat transfer coefficients. On the other hand, microchannels provide a large area of contact between the solid and coolant as well as a huge temperature gradient in the coolant near the channel wall due to the extremely small channel width. The prominent features of each technology concerned with the high heat transfer capabilities have allowed a variety of applications, while the main fields of applications have been distinguished from each other: the jet impingement has been widely used in industrial transport processes, while the microchannel cooling has been mainly employed in the cooling of microelectronic devices.

The increasing applications required for high-heat-flux treatments have drawn substantial improvement of each technology and expanded each field covering ground previously reserved for either one of these technologies. The use of jet impingement for the cooling of electronic components is an example of such infringement of the two competing technologies [3]. The competition between the two technologies has become unavoidable, thus requiring a systematic and objective comparison of the two technologies. This constitutes one of the main purposes of this study. That is a systematic comparison between jet impingement and microchannels, revealing which is more preferable for a given high-heat-flux application.

Performing a detailed comparison is quite difficult due to the multi-disciplinary characteristics of each of the involved technologies. The manufacturing cost, compactness and economic maintenance are also of importance in addition to the heat transfer characteristics. In some applications such as fusion reactors and synchrotrons, the heat transfer characteristics, however, are the most critical factor among all other considerations. In such cases, it is important to determine which technology provides a higher heat transfer capability. To this end, the thermal aspect serves as the primary one towards a comprehensive comparison. With this in mind, this work is aimed at providing criteria in selecting one technology over another in maximizing the heat transfer process. Based on the optimization procedures, the maximum heat flux attainable by each technology was evaluated within practical operation constraints, i.e. allowable

pressure drop and coolant flow rate. This is followed by a comparison of the heat transfer performance for the jet impingement and microchannel cooling technologies.

2. Multiple jet impingement

Jet impingement heat transfer has been studied extensively and continues to attract a good deal of attention due to its high heat transfer rates and its application in a variety of industries. When a jet impinges on a surface, very thin hydrodynamic and thermal boundary layers form in the impingement region owing to the jet deceleration and the resulting increase in pressure. Consequently extremely high heat transfer coefficients are obtained within the stagnation zone. Since the peak heat transfer is confined to the stagnation zone, a single jet impingement provides an effective means where highly localized heating or cooling is required. On the other hand, for applications with larger expanse of surface, multiple jet impingement can be applied.

With its prominent features such as high heat transfer, flexibility in design conditions, and a relatively simple configuration, jet impingement has been employed in a wide range of industrial processes and continues to broaden the scope of its application. Some examples include the annealing of metal, the tempering of glass, the drying of textiles, paper and film materials, and the cooling of gas turbine blades. In more recent applications, jet impingement has been used in the freezing of tissues in cryosurgery, the cooling of microelectronic components and neutron beam system.

Due to various industrial uses for impinging jets, extensive research has been conducted and a vast body of literature exists on this topic. The results from this research have been summarized in several comprehensive reviews. Historically, jet impingement research has primarily been concerned with gaseous jets and a review of the extensive literature published prior to 1976 has been provided by Martin [4]. Downs and James [5] also presented a literature survey on jet impingement heat transfer in which they focused on gas turbine component cooling. A related form of heat transfer by direct flame jet impingement has been reviewed by Viskanta [6].

Research on the liquid jet impingement has been substantiated with the increasing needs for high-heat-flux convective cooling as the heat transfer coefficient can be increased by several orders of magnitude compared to gaseous jet impingement. Two configurations are possible for the jet impingement with liquid as working fluid: submerged jets and free-surface jets. In the former case, a jet is discharged into stagnant fluid of the same type. In the latter, a liquid jet is exposed to a gaseous environment. Recently the research on both the submerged and free-surface liquid jet has been exhaustively reviewed by Webb and Ma [3].

In this study, our major concern is to evaluate practically attainable maximum heat flux by jet impingement. In this respect, the heat transfer characteristics of jet impingement are introduced briefly and the optimal design procedure is developed considering the crossflow effect. To this end, the focus is on the heat transfer by submerged liquid jet impingement due to its higher heat transfer coefficient as compared to the free-surface liquid or gaseous jet impingement [7].

2.1. Heat transfer in jet impingement

2.1.1. Flow and heat transfer characteristics of jet impingement

The flow field of an impinging jet can be divided into three separate regions, each with its distinct characteristics: the free jet region, the impingement region and the radial flow region as shown in Fig. 1. The flow in the free jet region is mainly in the axial direction and is not much affected by the presence of the impingement surface. Within this free jet region are two subregions, the potential core with velocity equal to the jet exit velocity and the lower-velocity shear layer, which results from the entrainment of the surrounding fluid. Downstream of the nozzle, the shear layer progressively grows and displaces the potential core, eventually reaching the jet centerline.

As the jet proceeds towards the impingement surface, it is influenced by this surface. This region constitutes the impingement region and is approximately 1.2 nozzle diameters away from the surface [4]. In this impingement region, the flow is decelerated in the axial direction and accelerated in the radial direction. The thickness of the boundary layer in this region is very thin and uniform due to the radial acceleration of the fluid. This results in a high heat transfer coefficient which is known to be proportional to $\sqrt{u/d}$ [8], where u is the axial velocity of the fluid entering the impingement region and d is the nozzle diameter.

When the nozzle-to-plate spacing is smaller than the potential core length, the axial velocity entering the impingement region is likely to be the same as the issuing velocity from the nozzle, resulting in a heat transfer coefficient which is nearly constant regardless of the

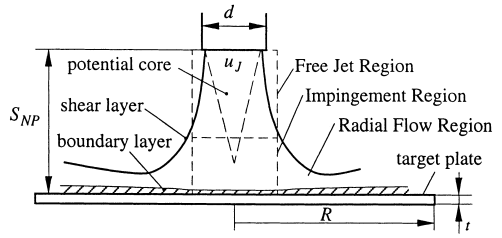

Fig. 1. Schematic of a typical jet impingement arrangement.

nozzle-to-plate spacing. However, at spacings larger than the length of the potential core, the velocity decreases with increasing spacing, resulting in a decrease of the heat transfer coefficient. In the radial flow region, as expected, the radial velocity decreases as it flows outward. This results in a thickening of the boundary layer and a gradual decrease in heat transfer coefficient along the radial direction.

It is known that the average heat transfer coefficient over the impingement surface depends on parameters such as $\sqrt{u_J/d}$, S_{NP}/d and R/d, where u_J, d, S_{NP} and R are defined in Fig. 1. In a review paper, Martin [4] elaborated the correlation equation for the average Nusselt number in a single jet impingement as follows:

$$\frac{Nu}{Pr^{0.42}} = G(d/R, S_{NP}/d)F(Re_J)$$

$$G(d/R, S_{NP}/d) = \frac{d}{R}\frac{1-1.1d/R}{1+0.1(S_{NP}/d-6)d/R}$$

$$F(Re_J) = 2Re_J^{1/2}\left(1+\frac{Re_J^{0.55}}{200}\right)^{0.5} \quad (1)$$

where Re_J and Nu are the Reynolds number and the Nusselt number based on the nozzle diameter:

$$Re_J = \frac{u_J d}{v}$$

$$Nu = \frac{hd}{k_f} \quad (2)$$

in which h is the average heat transfer coefficient based on the average temperature difference between the target and the coolant.

The correlation equation (1) is known to be valid in the range of

$$2000 \leqslant Re_J \leqslant 400\,000,$$
$$2.5 \leqslant R/d \leqslant 7.5,$$
$$2 \leqslant S_{NP}/d \leqslant 12. \quad (3)$$

2.1.2. Heat transfer by multiple jet impingement

The heat transfer for a multiple jet impingement can be inferred from the single jet impingement case by taking a representative area attributed to one jet among the multiple jet region. If the interaction between adjacent jets is negligible within the representative area and the spent fluid flows outward freely, the heat transfer data inferred from a single jet can be approximately representative of the actual situation. In this respect, the relative nozzle area, α_J, is defined a the ratio of the nozzle exit cross section to the surrounding area corresponding to a single jet, A_{corr}:

$$\alpha_J = \frac{\pi d^2/4}{A_{corr}}. \quad (4)$$

The surrounding area corresponding to a single jet, A_{corr}, depends on the nozzle-to-nozzle separation distance, S_{NN},

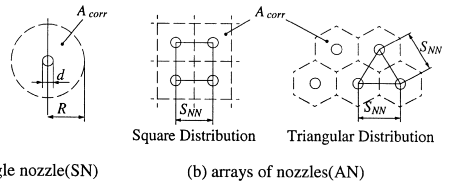

Fig. 2. Spatial arrangement of nozzles in regularly spaced arrays: (a) single nozzle (SN); (b) arrays of nozzles (AN).

and the spatial arrangement of nozzles as shown in Fig. 2. Figure 2 shows a single nozzle arrangement and two typical arrangements for multiple nozzles. Various expressions for the relative nozzle area, α_J, are listed in Table 1 for single nozzles and regularly spaced arrays of nozzles.

The correlation equation for the array of nozzles may be obtained from the single nozzle equation by replacing R/d with a term related to the relative nozzle area, α_J. From the first column of Table 1, this term is obtained as $1/\sqrt{4\alpha_J}$. The geometric function, G, for the arrays of nozzles thus becomes

$$G(\alpha_J, S_{NP}/d) = 2\sqrt{\alpha_J}\frac{1-2.2\sqrt{\alpha_J}}{1+0.2(S_{NP}/d-6)\sqrt{\alpha_J}}. \quad (5)$$

Equation (5) accounts for the effect of the nozzle to nozzle spacing, S_{NN}. However, the influence of nozzle-to-plate spacing, S_{NP}, also needs to be accounted for. This is done by noting that this simple replacement gives a sufficiently accurate result as long as the relative nozzle-to-plate distance, S_{NP}/d, remains below a certain limiting value, $(S_{NP}/d)_{lim}$. For larger distances, $S_{NP}/d > (S_{NP}/d)_{lim}$, the transfer coefficients for arrays of nozzles decrease more rapidly with S_{NP}/d than the corresponding single nozzle values. This is due to the interaction between adjacent jets in the multiple jet impingement arrangement, namely, a jet issuing from a nozzle loses its vigor prior to the impingement on the surface due to this interaction, which results in the decrease of heat transfer. When the jets are more closely distributed, the chance of interaction becomes larger and the heat transfer coefficient thus begins to decrease for a smaller nozzle-to-plate spacing. Consequently the limiting distance can be expressed as a function of the relative nozzle area, α_J, and is empirically found as [4]

Table 1
Relative nozzle area α_J

Single nozzle	AN (square)	AN (hexagon)
$\frac{1}{4}\left(\frac{d}{R}\right)^2$	$\frac{\pi}{4}\left(\frac{d}{S_{NN}}\right)^2$	$\frac{\pi}{2\sqrt{3}}\left(\frac{d}{S_{NN}}\right)^2$

$$(S_{NP}/d)_{lim} = 0.6/\sqrt{\alpha_J}. \quad (6)$$

The degradation of the heat transfer due to the interaction between the adjacent jets can be implemented into the single jet equation by an empirical correction function, K, based on the ratio of S_{NP}/d to its limiting value, $(S_{NP}/d)_{lim}$:

$$K\left(\frac{S_{NP}/d}{0.6/\sqrt{\alpha_J}}\right) = \begin{cases} 1, & \dfrac{S_{NP}/d}{0.6/\sqrt{\alpha_J}} \leqslant 1 \\ \left(\dfrac{S_{NP}/d}{0.6/\sqrt{\alpha_J}}\right)^{-0.3}, & \dfrac{S_{NP}/d}{0.6/\sqrt{\alpha_J}} \geqslant 1. \end{cases} \quad (7)$$

The discontinuous description of the array correction function, K, may be replaced by a single expression given by

$$K(S_{NP}/d, \alpha_J) = \left[1 + \left(\frac{S_{NP}/d}{0.6/\sqrt{\alpha_J}}\right)^6\right]^{-0.05}. \quad (8)$$

The function, F, given in equation (1) which describes the effect of the Reynolds number is prescribed for single jet impingement and has a different form for multiple jet impingement arrangement. The Reynolds function, F, for arrays of nozzles is empirically correlated by

$$F(Re_J)_{AN} = 0.5 Re_J^{2/3}, \quad 2000 < Re_J < 100\,000. \quad (9)$$

The foregoing modifications to the correlation equation for single nozzles result in an expression for the heat transfer coefficient for an array of nozzles given as

$$\left(\frac{Nu}{Pr^{0.42}}\right)_{AN} = K(S_{NP}/d, \alpha_J) G(S_{NP}/d, \alpha_J) F(Re_J)_{AN}$$
$$= \left[1 + \left(\frac{S_{NP}/d}{0.6/\sqrt{\alpha_J}}\right)^6\right]^{-0.05} \times \frac{\sqrt{\alpha_J}(1 - 2.2\sqrt{\alpha_J})}{1 + 0.2(S_{NP}/d - 6)\sqrt{\alpha_J}} Re_J^{2/3} \quad (10)$$

which is valid in the range of

$$2000 \leqslant Re_J \leqslant 100\,000,$$
$$0.004 \leqslant \alpha_J \leqslant 0.04,$$
$$2 \leqslant S_{NP}/d \leqslant 12.$$

2.1.3. Influence of spent flow

As mentioned earlier, the foregoing considerations for heat transfer in multiple jet impingement are for the case where the spent fluid can flow freely outward after impingement. This situation is found when the spent fluid flows directly outward through the impingement surface exits [9] or upward through outlets between the nozzles [10]. However without these particular treatments, the spent fluid is usually forced to flow laterally over the target plate. In this case, the outlet stream of the spent fluid (hereafter referred to as crossflow) may significantly influence the whole flow field and consequently the temperature field.

The crossflow decreases the impingement heat transfer by deflecting the jet and dissipating the impinging momentum. However the complexity involved in the phenomena precludes the advent of an adequate correlation equation describing the effect of crossflow. The crossflow elongates the footprint of the jet in the direction of the crossflow and thus the heat transfer from the surface to a jet or vice versa, is no longer axisymmetric [11, 12]. The velocity distribution of the crossflow is usually nonuniform in between the jets and consequently the flow field becomes three-dimensional [13]. In addition, the issuing velocity of each jet might differ between jets due to the existence of the crossflow [14].

As mentioned earlier, the influence of the crossflow prevents a comprehensive correlation equation describing its effect at this time. However there have been various works dealing with this subject and the outcome of previous works though fragmentary can be summarized as follows:

- the effect of interaction depends on u_c/u_J as well as S_{NP}/d, S_{NN}/d and Re_J where u_c is crossflow velocity,
- the effect of crossflow increases as u_c/u_J increases or S_{NP}/d decreases,
- when the average velocity of the crossflow is fixed, the distribution of the crossflow between the adjacent jets becomes more nonuniform as S_{NN}/d increases and S_{NP}/d decreases, and
- the heat transfer might be enhanced due to the crossflow itself when S_{NP} is very small.

Based on previous experimental investigations [13–17], it can be concluded that the effect of crossflow is negligibly small when

$$\frac{S_{NP}}{d}\frac{u_c}{u_J} < 0.1. \quad (11)$$

In order to assess the criteria for the jet arrangement parameters, such as S_{NP}/d, S_{NN}/d and R/d (where R is the radius of the target plate) with which the crossflow effect is negligible, and determine under what circumstances the multiple jet configuration produces an approximately uniform jet distribution, it is necessary to obtain the velocity distribution within the flow channel between the target and nozzle plates. To simplify the analysis it is assumed that the pressure and the velocity of crossflow are functions of the radius only. Furthermore, to assess the conditions which produce a uniform jet distribution, the fluid is considered to issue continuously from the entire area of the nozzle plate instead of issuing from distributed nozzles. The artificial velocity u_J^* of the fluid issuing uniformly from the nozzle plate, is represented by

$$u_J^* = \alpha_J u_J. \quad (12)$$

In addition, the pressure loss due to the friction at the channel wall is assumed to be relatively small as compared to the pressure drop due to the flow acceleration. Based on these assumptions, the continuity and momen-

tum equations integrated across the cross section reduce to

continuity equation

$$u_J^* = \frac{S_{NP}}{r}\frac{d}{dr}(ru_c) \tag{13}$$

momentum equation

$$\frac{1}{r}\frac{d}{dr}(ru_c^2) = -\frac{1}{\rho}\frac{dp}{dr} \tag{14}$$

where r is the radial coordinate of the target plate with its origin at the geometric center of the target plate. In addition, the jet velocity can be related to the pressure difference between the plenum where the jet originates and any radial location in the channel based on using an orifice discharge equation as

$$u_J = C_D[2(p_0 - p)/\rho]^{1/2}. \tag{15}$$

Eliminating u_J^* in equation (13) and using equations (12), (14) and (15) yields a differential equation for the crossflow velocity, u_c:

$$\frac{d}{dx}\left\{\frac{1}{x}\frac{d(xu_c)}{dx}\right\}^2 - \frac{2\varepsilon}{x}\frac{d(xu_c^2)}{dx} = 0 \tag{16}$$

where $x = r/R$, $\varepsilon = (\alpha_J C_D R/S_{NP})^2$ and R is the shortest length over which the fluid issued at the center of the target plate leaves the plate. This translates to the radius of the plate for a circular target and half the width of the plate for a square target.

Utilizing a perturbation method in equation (16) based on expanding u_c in terms of the perturbation parameter, ε, the variation of the crossflow velocity is obtained as

$$u_c = \frac{\dot{V}}{2\pi R S_{NP}}\left[\frac{r}{R} + \frac{3}{16}\varepsilon\left\{\left(\frac{r}{R}\right)^3 - \left(\frac{r}{R}\right)\right\} + \frac{1}{16^2}\varepsilon^2\left\{4\left(\frac{r}{R}\right)^5 - 9\left(\frac{r}{R}\right)^3 + 5\left(\frac{r}{R}\right)\right\} + \ldots\right] \tag{17}$$

where $\dot{V}$ is the coolant flow rate. Using equation (17) in equation (13) and subsequently in equation (12) results in an expression for the jet velocity distribution as

$$u_J = \frac{\dot{V}}{\pi R^2 \alpha_J}\left[1 + \frac{3}{16}\varepsilon\left\{2\left(\frac{r}{R}\right)^2 - 1\right\} + \frac{1}{16^2}\varepsilon^2\left\{12\left(\frac{r}{R}\right)^4 - 18\left(\frac{r}{R}\right)^2 + 5\right\} + \ldots\right]. \tag{18}$$

To obtain an approximately uniform cooling over the target plate, the jet velocity should be approximately independent of the nozzle location. To satisfy this condition a criterion for ε is assessed based on equation (18) as

$$\frac{3}{16}\varepsilon < 0.1 \quad \text{or} \quad \varepsilon < 0.5. \tag{19}$$

Equation (19) results in a criterion for nozzle-to-plate spacing, S_{NP}, as

$$S_{NP} > \sqrt{2}\alpha_J C_D R. \tag{20}$$

The crossflow velocity is largest at the edge of the target plate and thus the effect of crossflow should be largest there. Referring to equations (17) and (18), and evaluating them at $r = R$ yields the ratio of jet to crossflow velocities at the edge of the target plate as

$$\left.\frac{u_J}{u_c}\right|_{r=R} = \frac{2S_{NP}}{\alpha_J R}\left(1 + \frac{3}{16}\varepsilon - \frac{1}{16^2}\varepsilon^2 + \ldots\right). \tag{21}$$

Substituting equation (21) along with equation (19) in equation (11) yields the following criterion:

$$d > 5\alpha_J R. \tag{22}$$

The criterion given by equations (20) and (22) produces an approximately uniform jet distribution over the target plate with negligible influence from the crossflow.

2.2. Optimal configuration for multiple jet impingement

In the design of a multiple jet impingement cooling system, it is important to determine pertinent parameters such as the nozzle diameter, d, nozzle-to-nozzle separation, S_{NN}, and nozzle-to-plate spacing, S_{NP}, so as to maximize the heat removal from the heat source. Since increasing the coolant flow rate or impingement pressure always increases the heat removal, the pumping power would be used as a constraint when determining optimal values of the pertinent parameters for maximizing the heat removal process. It should also be noted that the correlation equation (10) shows that the decrease of nozzle-to-plate spacing, S_{NP}, always increases the heat transfer coefficient and thus there does not seem to exist an optimal value of the nozzle-to-plate spacing. However, since the nozzle-to-plate spacing impacts the crossflow, the optimal value of the nozzle-to-plate spacing is determined as its minimum value at which the crossflow effect is negligible.

Therefore the optimization procedure begins with obtaining the optimal values of S_{NN}/d and S_{NP}/d with the constraints placed on the pumping power and nozzle-to-plate spacing while attaining a negligible crossflow effect. The criterion for negligible crossflow effect is then applied to find a reasonable nozzle-to-plate spacing. To perform the optimization procedure, the mean nozzle exit velocity is first expressed as a function of the pumping power per unit area of target surface, P_0. To this end, P_0 can be expressed as

$$P_0 = \Delta p \dot{V}/A. \tag{23}$$

In the above expression, Δp and $\dot{V}$ are the pressure difference and total flow rate respectively and can be represented as

$$\Delta p = \xi(\rho/2)u_J^2, \quad \dot{V} = u_J \alpha_J A \tag{24}$$

in which u_J is the nozzle exit velocity averaged over the nozzles and ξ is the pressure loss coefficient. The pressure loss coefficient, ξ, can be taken as a constant regardless of the flow velocity within the operating range. Using equations (23) and (24), the flow velocity can be expressed as

$$u_J = \left(\frac{2P_0}{\xi\rho\alpha_J}\right)^{1/3}. \tag{25}$$

Noting that the nozzle-to-plate spacing is constant, and replacing u_J in equation (10) with that given by equation (25) results in

$$\frac{(hS_{NP}/k_f)/Pr^{0.42}}{[\{2P_0/(\xi\rho)\}^{1/3}S_{NP}/v]^{2/3}} = G_P(\alpha_J, S_{NP}/d)$$

where

$$G_P(\alpha_J, S_{NP}/d) = \frac{(S_{NP}/d)^{1/3}}{\alpha_J^{2/9}}\left[1+\left(\frac{S_{NP}/d}{0.6/\sqrt{\alpha_J}}\right)^6\right]^{-0.05} \times \frac{\sqrt{\alpha_J}(1-2.2\sqrt{\alpha_J})}{1+0.2(S_{NP}/d-6)\sqrt{\alpha_J}}. \tag{26}$$

The optimal arrangement maximizing the transfer coefficient for a given pumping power can be calculated from equation (26) by using

$$\frac{\partial G_P}{\partial(S_{NP}/d)} = 0 \quad \text{and} \quad \frac{\partial G_P}{\partial\alpha_J} = 0. \tag{27}$$

It should be noted the first optimization is done with respect to S_{NP}/d and not S_{NP} which is taken as a constant. These lead to the optimal arrangement obtained as

$$\alpha_{J\,opt} = 0.0152, \quad (S_{NP}/d)_{opt} = 5.43. \tag{28}$$

To complete the optimization procedure, it is necessary to determine the nozzle-to-plate spacing for negligible crossflow effect. Utilizing equations (22) and (28), the criterion for nozzle-to-plate spacing for significant crossflow effect is obtained as

$$S_{NP} > 5(S_{NP}/d)_{opt}\alpha_{J\,opt}R. \tag{29}$$

Comparing equation (29) with equation (20), the condition given by equation (29) is found to be more restrictive, and therefore it is the one that will be used to determine the optimal nozzle-to-plate spacing.

The maximum heat flux for an optimal multiple jet impingement arrangement can be written as

$$q_{J\,max} = \frac{k_f}{d_{opt}}Nu\Delta T \tag{30}$$

where ΔT is the temperature difference between the target plate and the coolant. Figure 3 shows the maximum heat removal from a square heat source plate utilizing an optimal arrangement for the nozzle arrays. The solid lines in the figure, which represent the maximum heat removal within the limit of negligible crossflow effect, are obtained using equations (30), (10), (28) and (29). The coolant is taken to be water and the temperature difference is set at

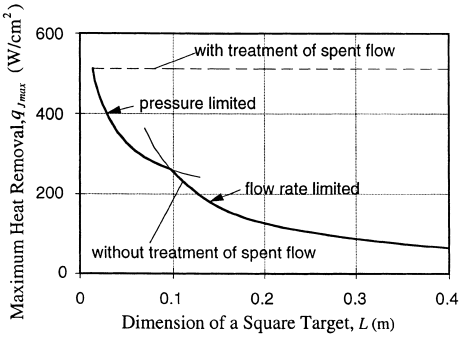

Fig. 3. Maximum heat flux from a square target plate using a multiple jet impingement cooling ($t = 0$ m, $\Delta T = 50$°C, $T_{f,out} - T_{f,in} > 3$°C and $\Delta p < 200$ kPa).

50°C which can be considered to be representative for different applications. The coolant flow rate is limited so as to maintain the coolant temperature difference between the inlet and outlet as 3°C since an excessively large flow rate necessitates an oversized circulation system even though it can increase the heat flux from the surface. Also the pressure load is limited to 200 kPa since the impingement pressure is already very large for a small nozzle diameter and a given coolant flow rate. Variation in the operating conditions can be explored with the cited set of equations. These variations did not have a significant effect on the presented conclusions.

As can be seen in Fig. 3, the thermal performance of the jet impingement is limited by the pressure condition for a smaller target plate, while restricted by the flow rate condition for a larger target plate. It is also found that the maximum heat flux extractable from a target plate decreases when increasing the extent of the target plate. This is because a larger target plate leads to a larger nozzle-to-plate spacing as well as a larger nozzle diameter. This can be seen through the use of equations (29) and (28) respectively. For jet arrays with favorable spent flow conditions such as those proposed by Hollworth and Dagan [9] or Huber and Viskanta [10], there is no need of limiting the nozzle-to-plate spacing. With proper treatment of spent flow, the maximum heat flux does not have to depend on the size of target plate. In this case, a smaller nozzle-to-plate spacing satisfying the optimal nozzle arrangement of equation (28) gives a higher thermal performance regardless of the extent of the target plate. It should be noted that the nozzle-to-plate spacing cannot be made smaller without a limit because a smaller nozzle-to-spacing accompanies a smaller nozzle diameter which necessitates more precise machining. When the nozzle diameter is set to be 0.5 mm, which is considered to be close to the limiting factor for machining a nozzle diameter, the corresponding heat flux attainable is shown as a broken line in Fig. 3. In this case, the maximum

allowable pressure difference through the nozzle is also limited to be 200 kPa.

3. Microchannel cooling

The microchannel cooling is a more recent technology as compared to that of the jet impingement cooling. One of the early citations of the concept of the microchannel cooling was made by Tuckerman and Pease [18]. Their work was aimed at the design of a compact heat sink with particular application for very-large-scale integrated (VLSI) circuits. They found that the heat transfer coefficient scales inversely with channel width for laminar flow in confined channels. Utilizing this idea they showed that conventional heat exchanger technology could be scaled down to tens of micrometers and applied directly to heat removal from VLSI circuits.

The basic concept of the microchannel cooling is illustrated in Fig. 4. Fins of large aspect ratio are located on one side of the target surface, while the coolant is driven through the space in between the fins. This microstructure provides a large area of contact between the solid and the fluid as well as a large temperature gradient within the fluid near the channel wall due to the extremely small channel width. Based on their optimization procedure, Tuckerman and Pease constructed a heat sink by etching the backside of a silicon wafer of 1 cm by 1 cm and achieved a heat flux of 790 W cm^{-2} with a temperature rise of 71°C using water as the coolant.

Since the work of Tuckerman and Pease [18], many investigations have been performed for evaluating the performance and feasibility of using microchannels for cooling of small target areas. As an example, Mahalingam [19] constructed a microchannel heat sink within a silicon substrate. The channels were about 200 μm wide with a depth of 1700 μm, separated by a 100 μm fin and a water flow rate of 12 $cm^3\ s^{-1}$ yielding a thermal resistance 0.03°C W^{-1}.

Kishimoto and Ohsaki [20] worked on a packaging technique wherein VLSI chips were mounted on a multilayered alumina substrate. Coolant channels (800 μm wide by 400 μm high) were made within the substrate at a staggered pitch of 2.54 mm leading to a thermal resistance of 0.31°C W^{-1} for a pressure drop of 19.6 kPa and a flow rate of 1 l min^{-1}.

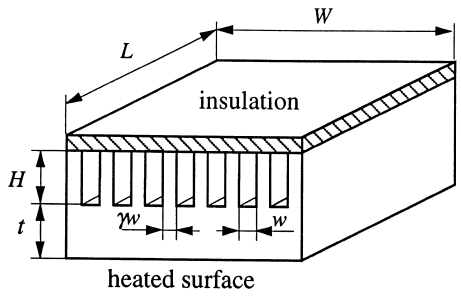

Fig. 4. Schematic of a microchannel cooling system.

The practical application of the microchannel cooling is restricted by the ability for machining microstructures. Meanwhile, additional studies on the optimization of the microchannel cooling have been conducted to determine the channel height, width and spacing that would yield the maximum thermal performance. Since the original work of Tuckerman and Pease [18] was subject to several constraints such as fully developed and laminar flow, fixed fin width ratio and constant fin efficiency, works by other researchers have concentrated on the exclusion of such constraints and better design of the microchannel cooling system. In this respect, the works of Samalam [21] and Knight et al. [22] are noteworthy.

Samalam [21] analyzed laminar heat transfer in microchannels theoretically without assuming a uniform temperature at a channel cross section and he obtained an optimal configuration for the case under consideration. With this optimal configuration it was shown that the thermal resistance can be lowered by 30% compared to that obtained by Tuckerman and Pease [18]. More recently Knight et al. [22] reported a comprehensive design method for microchannel heat sinks in which both laminar and turbulent flow regimes were considered. For the case presented, it was shown that a smaller thermal resistance can be obtained in the turbulent flow regime as compared to the laminar flow case for the same pressure load (but with different channel dimensions).

In this study, the feasibility of using microchannels for cooling larger surface areas is considered. Most applications which utilize microchannels are related to the use of compact heat sinks for high density electronic devices such as VLSI chips. Applications for larger surface areas are quite rare. Recent advances in precision machining technology such as EDM (Electrical Discharge Machining) may enable the manufacturing of the microstructures within a larger scale. Therefore, it is meaningful to investigate the feasibility of microchannels for cooling of a larger surface area.

In heat removal applications from a large surface area, the channel width should be larger than that for chip cooling to accommodate a reasonable pressure drop. Thus this decreases the maximum attainable heat transfer. In this work, the importance of the target plate dimension on the maximum heat flux removal attainable is also established.

3.1. Heat transfer in microchannels

As shown in Fig. 4, the microchannel cooling system consists of a series of channels and fins extending from one side of a heated target (heat source) plate. The heat transfer performance of a microchannel can be measured

by its thermal resistance $\Delta T/Q_M$, where ΔT is the temperature rise of the heated target plate above the input coolant temperature and Q_M is the extracted heat from the microchannel. In general, the thermal resistance is the sum of the following terms: the conductive resistance through the substrate between the heated target plate and the microchannel, the conductive resistance for the fin, the convective resistance between microchannel walls and the coolant fluid, and the capacitance resistance along the channel caused by the temperature rise of the fluid as it absorbs energy passing through microchannels. While the conduction resistance through the substrate increases with an increase in the substrate thickness, a minimum thickness is required to maintain the structural strength and thus the extent of this thickness does not enter into the thermal design considerations. Therefore, convective and conductive resistances for the fin and capacitance resistance along the channel will be the main factors for designing high-performance microchannels. To this end, the heat transfer in microchannels with a negligibly thin substrate is analyzed in this section, and the effect of the substrate thickness will be considered separately later on.

The convective and conductive resistances depend mostly on the geometry of the channel whereas the capacitance resistance is related to the coolant flow rate. Though the capacitance resistance can be lowered by increasing the flow rate, the pressure loss would also increase with an increase in the flow rate. Since the pressure loss is very large due to the micro nature of channels, it usually restricts the practical range of the operation of the microchannel cooling system. Thus the major concern in design of microchannel cooling systems is the geometrical prescription of the microchannel which would yield minimum thermal resistance with an acceptable pressure loss. For a given fin material and fixed dimension of the target plate, the thermal resistance, q, can be represented in a nondimensional form as

$$\theta = \frac{k_s L \Delta T}{Q_M}. \tag{31}$$

The heat transfer in microchannels with a negligibly thin substrate can be analyzed with a simple model in which the coolant flows through narrow rectangular channels separated by fins with an imposed constant heat flux at the fin base. In this situation, the typical temperature distribution in microchannels along the L direction (Fig. 4) are likely to be as those shown in Fig. 5.

Since the conduction resistance in the substrate is insignificant for a negligibly thin substrate, the maximum temperature difference between the target plate and coolant can be divided into two components, i.e. $\Delta T_{(\mathrm{conv+cond}),\mathrm{fin}}$ and ΔT_{cap} which denote the temperature differences due to the convective and conductive resistances of the fin and the capacitance resistance along the channel, respectively. The two thermal resistances are rendered dimensionless using each of the corresponding temperature differences and equation (31). This yields

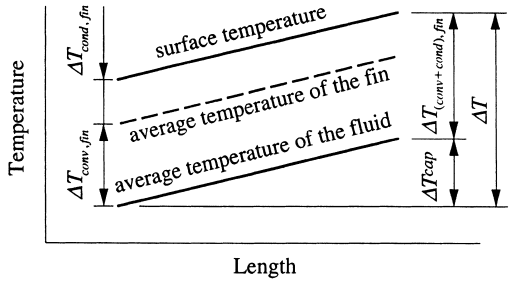

Fig. 5. Temperature distribution in a microchannel.

$$\theta = \frac{k_s L \Delta T_{(\mathrm{conv+cond}),\mathrm{fin}}}{Q_M} + \frac{k_s L \Delta T_{\mathrm{cap}}}{Q_M} = \theta_{(\mathrm{conv+cond}),\mathrm{fin}} + \theta_{\mathrm{cap}}. \tag{32}$$

The average temperature of the fin is not the same as the base temperature due to the finite fin conductivity. Thus the average temperature difference between the fluid and the fin is always smaller than the temperature difference between the surface and the fluid as shown in Fig. 5. To account for the finite fin conductivity, the fin efficiency, h, is introduced and the heat transfer through the fin is expressed by

$$Q_M = hLW\alpha_M \eta \Delta T_{(\mathrm{conv+cond}),\mathrm{fin}} \tag{33}$$

where α_M is an area enlargement factor and is defined as the ratio of the total surface area of the channel walls in contact with the fluid to the surface area of the target plate. That is

$$\alpha_M = \frac{2(H/w+1)}{1+\gamma}. \tag{34}$$

Substituting equations (33) and (34) into equation (32) yields an expression for the convective and conductive resistance of the fin:

$$\theta_{(\mathrm{conv+cond}),\mathrm{fin}} = \frac{\kappa}{Nu}\frac{H}{W}\frac{\omega^2(1+\gamma)}{\eta} \tag{35}$$

where

$$\kappa = \frac{k_s}{k_f}, \quad Nu = \frac{h d_h}{k_f}, \quad \omega = \frac{d_h}{2H} \tag{36}$$

and d_h is the hydrodynamic diameter of the channel, defined as $d_h = 2wH/(w+H)$. When the aspect ratio of the channel, w/H is very small, which is usually the case in microchannels, the hydrodynamic diameter is approximated as $d_h \approx 2w$, thus $\omega \approx w/H$.

An analytical approximation for the fin efficiency, h, can be obtained by assuming a constant heat transfer coefficient over the walls and modeling the heat flow in the walls as one-dimensional. This leads to

$$\eta = \frac{\tanh \lambda}{\lambda} \tag{37}$$

where

$$\lambda = \left(\frac{Nu}{\kappa}\right)^{1/2} \frac{1}{\omega\gamma^{1/2}}. \tag{38}$$

It should be noted that η is a monotonically decreasing function of $l\lambda$ with $\eta \approx 1$ for $\lambda \ll 1$ and $\eta \approx \lambda^{-1}$ for $\lambda \gg 1$. The heat transferred to the fluid can also be written as

$$Q_{\mathrm{M}} = \rho c_{\mathrm{P}} \dot{V} \Delta T_{\mathrm{cap}}. \tag{39}$$

The capacitance resistance can then be written as

$$\theta_{\mathrm{cap}} = \frac{k_{\mathrm{s}} L}{\rho c_{\mathrm{P}} \dot{V}} = \frac{2\kappa}{Pr} \frac{L}{W} \frac{\omega(1+\gamma)}{Re_{\mathrm{M}}} \tag{40}$$

where Re_{M} is the Reynolds number based on the hydrodynamic diameter of the channel:

$$Re_{\mathrm{M}} = \frac{u d_{\mathrm{h}}}{v}. \tag{41}$$

As discussed previously, the coolant flow is limited by the existence of a maximum imposed pressure. The relation between the fluid velocity and the corresponding pressure loss is represented by the friction factor. The definition of the friction factor is expressed in terms of nondimensional parameters as

$$f = \frac{\Delta p d_{\mathrm{h}}/L}{2\rho u^2} = \left(\frac{H}{L}\right)^3 \frac{4P}{Re_{\mathrm{M}}^2} \omega^3 \tag{42}$$

where P is the nondimensional pressure loss defined as

$$P = \frac{(\Delta p/\rho)L^2}{v^2}. \tag{43}$$

The heat rate extractable from the heated target plate can then be found as

$$q_{\mathrm{M}} = k_{\mathrm{s}} \frac{\Delta T}{L} \frac{1}{\theta} \tag{44}$$

where q_{M} is the heat flux. The main emphasis in this work is based on the application of microchannels to heat sources with large surface areas. As such, the length of the channel becomes very large as compared to the hydrodynamic diameter of the microchannel. Thus the flow within the channel is essentially hydrodynamically and thermally fully developed. Since the flow condition in the channel can be either laminar or turbulent, two sets of correlation equations are required.

When the flow is laminar, the friction factor and the Nusselt number are determined only be the aspect ratio of the channel, w/H, and expressed as [22, 23]

$$f = \frac{4.70 + 19.64\Omega}{Re_{\mathrm{M}}} \tag{45}$$

$$Nu = -1.047 + 9.326\Omega \tag{46}$$

where W is a parameter defined in terms of the channel aspect ratio as

$$\Omega = \frac{(w/H)^2 + 1}{(w/H + 1)^2}. \tag{47}$$

If the flow is turbulent within the channel, the correlation equations for the friction factor and the Nusselt number can be obtained from [24]

$$f = \begin{cases} 0.079 Re_{\mathrm{M}}^{-0.25} & 10^4 < Re_{\mathrm{M}} < 4\times 10^4 \\ 0.046 Re_{\mathrm{M}}^{-0.2} & 4\times 10^4 < Re_{\mathrm{M}} < 10^6 \end{cases} \tag{48}$$

$$Nu = \frac{(Re_{\mathrm{M}} - 1000) Pr f/2}{1.0 + 12.7\sqrt{f/2}(Pr^{2/3} - 1)}, \quad 2300 < Re_{\mathrm{M}} < 5\times 10^6, \quad 0.5 < Pr < 2000. \tag{49}$$

Once the Nusselt number and friction factor are known as functions of the Reynolds number, the convective and conductive resistances of the fin and the capacitance resistance are evaluated from equations (35), (40), (42) and depending on whether the flow is laminar or turbulent from equations (45), (46) or (48), (49), respectively. Figure 6 shows that the variation of the heat flux extractable from an aluminum target plate which has dimensions of $L = W = 0.1$ m with $\Delta T = 50^{\circ}$C and $\Delta P = 200$ kPa when the ratio of the channel height to the plate dimension, H/L, is 0.02. These operating conditions can be considered to be representative for several different applications. It should be noted that variations in these operating conditions did not have a significant effect on the presented conclusions.

It can be seen that the flow is laminar for a small ω but becomes turbulent when ω becomes larger than 0.06. This is because increasing ω implies an increase in the hydrodynamic diameter which results in an increase in the coolant flow rate for a fixed pressure loss and thus an increase in the Reynolds number. It is also seen that the heat flux increases with an increase of ω for a small ω until it reaches its maximum value around $\omega = 0.15$, after which it decreases with further increase in ω. This is due to the fact that the total thermal resistance is the sum of the two resistances which have different dependence on ω: the convective and conductive resistances of the fin increase with an increase in ω while the capacitance resist-

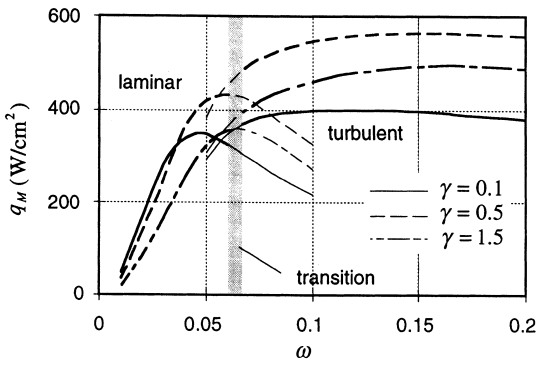

Fig. 6. Heat flux extractable from a square target plate utilizing microchannels ($L = W = 0.1$ m, $H/L = 0.02$ with $\Delta T = 50^{\circ}$C and $\Delta p = 200$ kPa).

ance decreases with an increase in ω. Therefore, there exists an optimal ω at which the sum of two thermal resistances is minimum and the heat flux thus becomes maximum for a given dimension of target plate. The influence of the variation of γ is similar to that of ω and there also exists an optimal value for γ and as such is not presented here for brevity.

The optimal values of ω and γ and the resultant maximum heat flux also depend on the dimension of target plate and are evaluated in the following section.

3.2. Optimization of the channel geometry

In this section, an optimization procedure is introduced to obtain the optimal values of ω and γ and the resultant maximum heat flux in terms of the target plate dimensions. To emphasize the optimization procedure the target plate is taken as a square, i.e. $L = W$. For a large target plate of the order of 0.1 by 0.1 m, the optimal value of ω is quite small (see Fig. 6) and λ is sufficiently large, that the fin efficiency, η, can be approximated, using equations (37)and (38), as

$$\eta \approx \lambda^{-1} = (Nu/\kappa)^{-1/2}\omega\gamma^{1/2}. \tag{50}$$

Based on equations (45), (46), (48) and (49), the Nusselt number and the friction factor are represented in terms of a simple function of the Reynolds number as

$$f = c_1 Re_M^{-a_1} \tag{51}$$

$$Nu = c_2 Re_M^{a_2} \tag{52}$$

where the coefficients, c_1 and c_2, and the exponents, a_1 and a_2 vary according to the range of the Reynolds number. With the foregoing simplifications, the two resistances can be represented in terms of nondimensional pressure and geometric parameters as

$$\theta_{(\mathrm{conv+cond}),\mathrm{fin}} = \left(\frac{\kappa}{c_2}\right)^{1/2}\left(\frac{c_1}{4P}\right)^{\frac{1-m}{3}}\left(\frac{L}{H}\right)^{-m}\omega^m(1+\gamma)\gamma^{-1/2} \tag{53}$$

$$\theta_{\mathrm{cap}} = \frac{2\kappa}{Pr}\left(\frac{c_1}{4P}\right)^{\frac{1+n}{3}}\left(\frac{L}{H}\right)^{1+n}\omega^{-n}(1+\gamma) \tag{54}$$

where

$$m = 1-3a_2/(4-2a_1) \quad \text{and} \quad n = (1+a_1)/(2-a_1). \tag{55}$$

Equations (42), (43) and (50)–(52) were used in obtaining both equations (53) and (54) along with equation (35) in equation (53) and equation (40) in equation (54). For turbulent flow m ranges from 0.23 to 0.33 and n varies from 0.67 to 0.71 while m and n are 1 and 2 respectively for laminar flow. The optimal values of ω and γ for minimizing the total thermal resistance are calculated from

$$\frac{\partial\theta}{\partial\omega} = 0 \quad \text{and} \quad \frac{\partial\theta}{\partial\gamma} = 0 \tag{56}$$

where θ is given in equation (32). After some manipulation, the optimal values are obtained as

$$\gamma_{\mathrm{opt}} = n/(2m+n) \tag{57}$$

$$\omega_{\mathrm{opt}} = \left(\frac{2n\sqrt{c_2\kappa}}{mPr}\right)^{\frac{1}{m+n}}\left(\frac{L}{H}\right)^{1+\frac{1}{m+n}}\left(\frac{c_1}{4P}\right)^{1/3}\gamma_{\mathrm{opt}}^{1/2(m+n)} \tag{58}$$

The total thermal resistance for the optimal configuration is then obtained by using γ_{opt} and ω_{opt} in equations (53) and (54) and subsequently combining $\theta_{(\mathrm{conv+cond}),\mathrm{fin}}$ and θ_{cap} according to equation (32). This results in

$$\theta_{\min} = \frac{m+n}{nc_2}(c_2\kappa)^{\frac{2m+n}{2(m+n)}}\left(\frac{2n}{mPr}\right)^{\frac{m}{m+n}} \times \left(\frac{L}{H}\right)^{\frac{m}{m+n}}\left(\frac{c_1}{4P}\right)^{1/3}\gamma_{\mathrm{opt}}^{-[n/2(m+n)]}(1+\gamma_{\mathrm{opt}}) \tag{59}$$

$$q_{\mathrm{Mmax}} = k_s\frac{\Delta T}{L}\frac{1}{\theta_{\min}} \tag{60}$$

where equation (60) is obtained through using $\theta_{\min}$ in equation (44). The variation of the maximum heat flux extractable from a square heated aluminum plate with $\Delta T = 50^\circ$C and $\Delta p = 200$ kPa as a function of the channel height is shown in Fig. 7. It can be seen that the heat flux increases with H/L but the rate of increase is reduced with further increases in H/L. It is also shown that the heat flux decreases as the extent of the target plate increases. This is because the capacitance resistance increases as the microchannel becomes longer due to an increase in the plate surface area. The explicit dependence of the heat flux on the dimension of the target plate can be obtained by substituting equations (43) and (59) in equation (60). This results

$$q_{\mathrm{Mmax}} \sim \Delta p^{1/3}L^{-1/3}\left(\frac{H}{L}\right)^{\frac{m}{m+n}}. \tag{61}$$

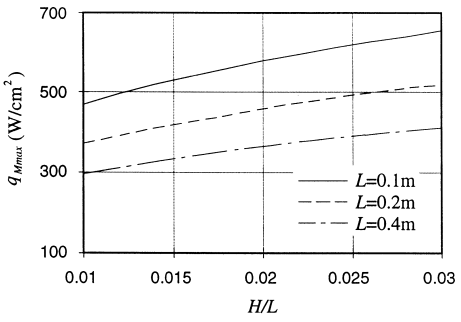

Fig. 7. Maximum heat flux extractable from a square target plate utilizing microchannels ($\Delta T = 50^\circ$C and $\Delta p = 200$ kPa).

It is worthy of note that the heat flux depends approximately on $(H/L)^{0.3}$, which implies that a 100% increase in the channel height will result in only a 25% increase in the attainable heat flux. This is due to the decrease in the fin effectiveness with increasing the channel height and should certainly be considered in the design considerations.

4. Comparison between jet impingement and microchannel cooling

In this part, the jet impingement cooling and microchannel cooling thermal performances are compared to each other. To this end, it is necessary to establish the conditions under which the comparison should be made. This is not a simple task as these technologies are fundamentally quite different from each other. The jet impingement cooling usually requires a very large coolant flow rate with a relatively small pressure drop, while the microchannel cooling is subject to a large pressure drop even when a relatively small coolant flow rate is used. Subsequently, a constant pressure drop condition would be preferable for the jet impingement while a constant coolant flow rate condition would be advantageous for the microchannel cooling. A constant pumping power condition in this case is likely to be unreasonable since only either an unacceptably high pressure drop with a small flow rate (for microchannel cooling), or an impracticably large flow rate with a small pressure drop (for jet impingement cooling) could yield a reasonable range for the pumping power. Therefore, either condition of the constant pressure drop, constant coolant flow rate or constant pumping power is not reasonable for comparison purposes.

As was mentioned earlier, however, the main interest in this study is to understand which technology will provide a higher heat transfer capability. Focusing on this point, the values of heat flux attainable with these two technologies are evaluated separately at their respective optimal operation conditions within a practical range of pressure drop and coolant flow rate, instead of being calculated at a given pressure drop or a given coolant flow rate.

When the heat is to be removed from the target plate, the heat is usually generated not at the external surface but immediately external to it. The conductive resistance through the finite thickness between the heated surface and external surface of the target plate would cause a considerable degradation in the heat transfer performance for both the jet impingement and microchannel cooling. Therefore, this factor should be taken into account when comparing the practically attainable heat transfer capabilities for each of these techniques. Considering the conductive resistance through the plate of thickness, t, as well as the convective cooling, the heat flux attainable by the jet impingement cooling can be written as

$$q_{\mathrm{J\,max}} = \frac{k_{\mathrm{f}}\Delta T/d_{\mathrm{opt}}}{1/Nu + (t/d_{\mathrm{opt}})/\kappa} \tag{62}$$

where Nu is the Nusselt number at the external surface and κ signifies the conductivity ratio of the plate to the coolant fluid. Comparing this equation with equation (30) for a negligibly thin plate, the thermal performance degradation of the jet impingement due to a finite thickness of the plate would be substantial even for a large Nusselt number if the conductivity ratio, κ, is small. In a similar manner, the heat flux attainable by attaching microchannels onto a target plate with a finite thickness, t, can be written as

$$q_{\mathrm{M\,max}} = \frac{k_{\mathrm{s}}\Delta T/L}{\theta_{\min} + (t/L)}. \tag{63}$$

This equation implies that the additional thermal resistance due to the finite thickness of the plate, which is not included in equation (60), is equal to t/L.

Figure 8 presents the comparison between the maximum heat flux extractable using jet impingement cooling and microchannel cooling.

In producing this set of figures, the coolant and the plate material are assumed to be water and aluminum respectively and the temperature difference is set to be 50°C. The maximum allowable pressure drop is 200 kPa and the coolant flow rate is limited so as to maintain the coolant temperature difference between the inlet and outlet larger than 3°C. These operating conditions can be considered to be representative for several different applications. Variations in these operating conditions did not produce a significant effect on the presented conclusions. In evaluating the jet impingement cooling characteristics, the ratio of the thickness to the length of the square plate, t/L is varied from 0 to 0.01. It should be noted that the thickness of the plate is usually increased with an increase in the extent of the surface in order to maintain the structural strength. In the case of microchannel cooling, this ratio t/L is also varied from 0 to 0.01 in the evaluation of cooling capability. It should be noted that for microchannel cooling a minimum thickness of the target plate which is attached to the microchannels is also required so as to sustain the imposed thermomechanical stresses. It is anticipated that this thickness would result at a minimum t/L of 0.005 but more likely this ratio should be 0.01. Finally, the ratio of the channel height to the target plate dimension, H/L, is set at an upper value of 0.01 considering the difficulties associated with manufacturing channel height ratios larger than this value. However, for informational purposes the heat removal variations for the microchannel cooling for $H/L = 0.02$ is also presented in Fig. 8. It can be seen that even at such a high setting the conclusions are essentially the same.

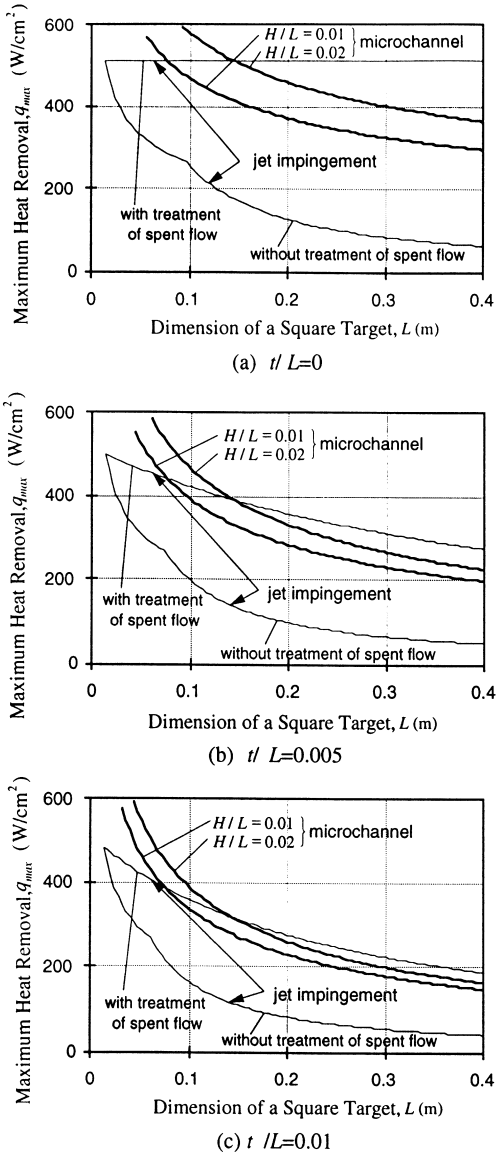

Fig. 8. Thermal performance comparison between the jet impingement and microchannel cooling ($\Delta T = 50°C$, $T_{f,out} - T_{f,in} > 3°C$ and $\Delta p < 200$ kPa): (a) $t/L = 0$; (b) $t/L = 0.005$; (c) $t/L = 0.01$.

As seen in Fig. 8, the heat transfer performance decreases significantly for both the jet impingement and microchannel cooling due to the conductive resistance through the plate as anticipated from equations (62) and (63). It should be noted that the maximum heat removal variation for the jet impingement with treatment of the spent flow is no longer constant as in Fig. 3 due to accounting of the conductive resistance of the target plate as cited earlier. The heat transfer degradation in this case increases with increasing the length of the plate and the maximum heat flux attainable is substantially reduced with an increase in the size of target plate. It can be seen that the degradation is also substantial in the case of microchannel cooling. Comparison of the three lines with different thickness ratios in Fig. 8 reveals the heat removal by microchannel cooling decreases significantly due to even a small increase in the plate thickness.

It is seen that the thermal performance of the jet impingement without any treatment of spent flow is substantially lower than that by the microchannel cooling regardless of the target plate dimension. With proper treatment of spent flow, however, the jet impingement is quite comparable to the microchannel cooling. For the same thickness ratio, the heat flux extractable by the jet impingement with treatment of spent flow becomes larger than that by the microchannel cooling for larger target dimensions while it is smaller for smaller target dimensions. Even if the thickness of the base plate in microchannel cooling can be reduced to half of the target plate thickness used in jet impingement case, the heat removal attainable by the jet impingement is still comparable to that by the microchannel cooling especially for target plate dimensions of the order of 0.07 by 0.07 m or larger.

Consequently, the microchannel cooling is preferable for a target dimension smaller than 0.07 by 0.07 m, while the jet impingement is quite comparable to or better than the microchannel cooling for a larger target plate if the spent flow is properly treated.

5. Conclusions

A comparative investigation and analysis have been performed for high heat flux applications between the jet impingement and microchannel cooling. These two technologies are fundamentally different and as such possess different operational conditions. The jet impingement cooling usually requires a very large coolant flow rate with a relatively small pressure drop, while the microchannel cooling is subject to a large pressure drop even for a relatively small coolant flow rate. Due to the large discrepancy in the operational conditions, it is unreasonable to compare the two technologies under the same set of conditions.

Therefore, the performances of the two technologies are compared at their individual optimal conditions in this work. To this end, the optimization procedure is developed first for each technology. Based on the optimization procedure, the maximum heat flux attainable by each technology was evaluated within a practical operation range, i.e. maximum pressure load and allowable coolant flow rate. This is followed by a comparison of the heat transfer performance of the jet impingement and microchannel cooling based on the attainable maximum heat flux.

Various qualitative and quantitative aspects of both jet impingement and microchannel cooling as well as the combined features of the two technologies were analyzed and presented in this work. Furthermore, the effects of target plate dimensions and thickness as well as some of the optimization conclusions have been presented for the first time. The analysis reveals that the thermal performance of the jet impingement without any treatment of spent flow is substantially lower than that by the microchannel cooling regardless of the target plate dimension. With proper treatment of spent flow, however, the jet impingement is quite comparable to the microchannel cooling. Specifically, the microchannel cooling is preferable for a target dimension smaller than 0.07 by 0.07 m, while the jet impingement is comparable or better than the microchannel cooling for a larger target plate if a proper treatment is applied for the spent flow after the impingement.

In selecting either of these two technologies, however, economic aspects, such as manufacturing and maintenance cost, also have to be taken into account, since the better performing one may not be necessarily the more suitable one.

Acknowledgements

The support provided by the Department of Energy under grant number DE-F602-93ER61612 and the support provided by the Korea Institute of Science and Technology is acknowledged and appreciated.

References

[1] M.G. Izenson, J.L. Martin, Optimal thermal-hydraulic performance for helium cooled divertors, Fusion Technology 29 (1996) 545–558.
[2] J.H. Rosenfeld, M.T. North, Porous media heat exchangers for cooling of high-power optical components, Optical Engineering 34 (2) (1995) 335–341.
[3] B.W. Webb, C.-F. Ma, Single-phase liquid jet impingement heat transfer, Advances in Heat Transfer 26 (1995) 105–217.
[4] H. Martin, Heat and mass transfer between impinging gas jets and solid surfaces, Advances in Heat Transfer 8 (1977) 1–60.
[5] S.J. Downs, E.H. James, Jet impingement heat transfer—a literature survey, ASME Paper No. 87-H-35, ASME, New York, 1987.
[6] R. Viskanta, Heat transfer to impinging isothermal gas and flame jets, Experimental Thermal and Fluid Science 6 (1993) 111–134.
[7] D.J. Womac, F.P. Incropera, S. Ramadhyani, Correlating equations for impingement cooling of small heat sources with multiple circular liquid jets, Journal of Heat Transfer 116 (1994) 482–486.
[8] F.M. White, Viscous Fluid Flow, McGraw-Hill, New York, 1974.
[9] B.R. Hollworth, L. Dagan, Arrays of impinging jets with spent fluid removal through vent holes on the target surface—Part 1: average heat transfer, ASME Journal of Engineering for Power 102 (1980) 994–999.
[10] A.M. Huber, R. Viskanta, Convective heat transfer to a confined impinging array of air jets with spent air exits, Journal of Heat Transfer 116 (1994) 570–576.
[11] D.E. Metzger, R.J. Korstad, Effects of crossflow on impingement heat transfer, Journal of Engineering for Power (1972) 35–41.
[12] K.W. Van Treuren, Z. Wang, P.T. Ireland, T.V. Jones, Detailed measurements of local heat transfer coefficient and adiabatic wall temperature beneath an array of impinging jets, Journal of Turbomachinery 116 (1994) 369–374.
[13] R.N. Koopman, E.M. Sparrow, Local and average transfer coefficients due to an impinging row of jets, International Journal of Heat and Mass Transfer 19 (1976) 673–683.
[14] L.W. Florschuetz, C.R. Truman, D.E. Metzger, Streamwise flow and heat transfer distributions for jet array impingement with crossflow, Journal of Heat Transfer 103 (1981) 337–342.
[15] D.M. Kercher, W. Tabakoff, Heat transfer by a square array of round air jets impinging perpendicular to a flat surface including the effect of spent air, Journal of Engineering for Power (1970) 73–82.
[16] N.T. Obot, T.A. Trabold, Impingement heat transfer within arrays of circular jets: Part 1—effects of minimum, intermediate, and complete crossflow for small and large spacings, Journal of Heat Transfer 109 (1987) 872–879.
[17] R.J. Goldstein, W.S. Seol, Heat transfer to a row of impinging circular air jets including the effect of entrainment, International Journal of Heat and Mass Transfer 34 (1991) 2133–2147.
[18] D.B. Tuckerman, R.F.W. Pease, High-performance heat sinking for VLSI, IEEE Electron Device Letters EDL-2 (5) (1981) 126–129.
[19] M. Mahalingam, Thermal management in semiconductor device packaging, Proceedings of IEEE 73 (1985) 1396–1404.
[20] T. Kishimoto, T. Ohsaki, VLSI packaging technique using liquid-cooled channels, 36th Electrics Components Conference Proceedings 1986, pp. 595–601.
[21] V.K. Samalam, Convective heat transfer in microchannels, Journal of Electronic Materials 18 (5) (1989) 611–617.
[22] R.W. Knight, D.J. Hall, J.S. Goodling, R.C. Jaeger, Heat sink optimization with application to microchannels, IEEE Transactions on Components, Hybrids, and Manufacturing Technology 15 (5) (1992) 832–842.
[23] A. Bejan, Convection Heat Transfer, John Wiley and Sons, 1984.
[24] W.M. Kays, M.E. Crawford, Convective Heat and Mass Transfer, 3rd ed., McGraw-Hill, 1993.